$NO_2 \cdots NO_2$ contacts under compression: testing the forces in soft donor-acceptor interactions.

Fabio Montisci[1*], Arianna Lanza[1,2,3], Nicola Casati[2], and Piero Macchi[1,4*]

[1]) Department für Chemie und Biochemie, Universität Bern, Bern, Switzerland
[2]) Swiss Light Source, Paul Scherrer Institute, Villigen, Switzerland
[3]) Center for Nanotechnology Innovation, Istituto Italiano di Tecnologia, Pisa, Italy
[4]) Dipartimento di Chimica, Materiali e Ingegneria Chimica "Giulio Natta", Politecnico di Milano, Milan, Italy

Abstract

Intermolecular forces and energies are not directly observable and cannot be retrieved from a crystal structure determination, which simply pictures the resulting equilibrium between forces. In this work, using compression to sample the repulsive part of potentials, we show that high pressure studies may give insight in the nature of intermolecular forces. We focus our attention on controversial $\pi^* \longleftarrow n$ interactions between NO_2 groups, which exhibit several conformations. Using XRD and *ab initio* calculations, we describe the high pressure behavior and phase transition of 4-amino-4′-nitrobiphenyl. To deepen our understanding on the nature of $NO_2 \cdots NO_2$ interactions we used several theoretical tools, including pairwise atomic potential energies and forces. The results show that this interaction is associated with a mild stabilization. Since the repulsive forces are experimentally found to be weaker than those of other contacts, we conclude that also the attractive forces are weak, although in excess of the repulsive ones.

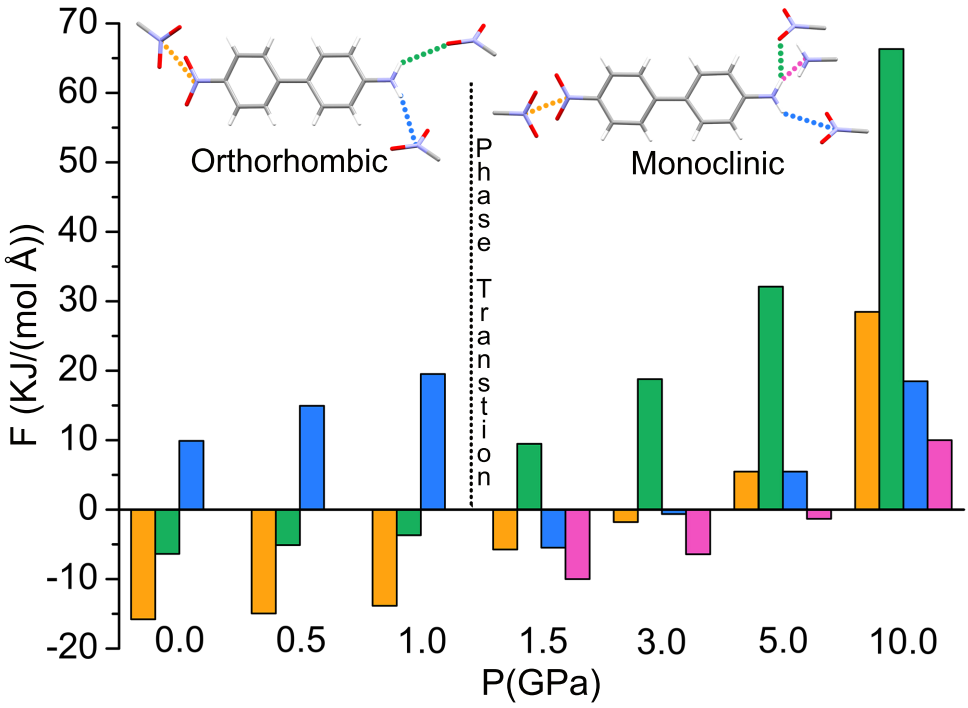

Forces of the main intermolecular interactions of 44′ANBP at different pressures, calculated with the semi-empirical atomic pairwise potential.

*Fabio Montisci, Department für Chemie und Biochemie, Universität Bern, Freiestrasse 3, 3012 Bern, Switzerland (CH),+41 031 631 4273, *fabio.montisci@dcb.unibe.ch*
*Piero Macchi, Department für Chemie und Biochemie, Universität Bern, Freiestrasse 3, 3012 Bern, Switzerland (CH), +41 031 631 4281, *piero.macchi@dcb.unibe.ch*
Dipartimento di Chimica, Materiali e Ingegneria Chimica "Giulio Natta", Politecnico di Milano, P.zza Leonardo da Vinci, 32 I-20133 Milan, Italy (I), *piero.macchi@polimi.it*.

$NO_2 \cdots NO_2$ contacts under compression: testing the forces in soft donor-acceptor interactions.

Fabio Montisci,[*,†] Arianna Lanza,[†,‡,¶] Nicola Casati,[‡] and Piero Macchi[*,†,§]

†*Department für Chemie und Biochemie, Universität Bern, Bern, Switzerland*

‡*Swiss Light Source, Paul Scherrer Institute, Villigen, Switzerland*

¶*Center for Nanotechnology Innovation, Istituto Italiano di Tecnologia, Pisa, Italy*

§*Dipartimento di Chimica, Materiali e Ingegneria Chimica "Giulio Natta", Politecnico di Milano, Milan, Italy*

E-mail: fabio.montisci@dcb.unibe.ch; piero.macchi@polimi.it

Phone: +41 031 631 4281

Abstract

Intermolecular forces and energies are not directly observable and cannot be retrieved from a crystal structure determination, which simply pictures the resulting equilibrium between forces. In this work, using compression to sample the repulsive part of potentials, we show that high pressure studies may give insight in the nature of intermolecular forces. We focus our attention on controversial $\pi^* \longleftarrow n$ interactions between NO_2 groups, which exhibit several conformations. Using XRD and *ab initio* calculations, we describe the high pressure behavior and phase transition of 4-amino-4′-nitrobiphenyl. To deepen our understanding on the nature of $NO_2 \cdots NO_2$ interactions we used several theoretical tools, including pairwise atomic potential energies and forces. The results show that this interaction is associated with a mild stabilization. Since the

repulsive forces are experimentally found to be weaker than those of other contacts, we conclude that also the attractive forces are weak, although in excess of the repulsive ones.

Introduction

Weak intermolecular interactions play a crucial role in crystal engineering, but they are also relevant for as diverse topics as physical organic chemistry, drug design, structural biology, enzymatic reactions, and supramolecular chemistry. The best known and characterized of such interactions is of course the hydrogen bond (HB), which displays a rather varied nature and strength.[1] Recently also the so called "halogen",[2] "chalcogen",[3] "pnicogen",[4,5] and even "carbon" bonds,[6] so named for analogy with the HB, have aroused growing interest. At present, other kinds of weaker interactions have not been so profoundly investigated. However, for a deep understanding of the effect of intermolecular interactions on material properties, there is a strong need of simultaneously comparing different interactions and establishing their hierarchy.

Every molecule in a crystal is subject to stabilizing or destabilizing interactions with the neighboring molecules, but the information obtained with a crystallographic structure determination only depicts an average configuration of the final equilibrium, and attractive or repulsive forces and stabilizing or destabilizing energies are experimentally undetectable. For this reason, the role of weak intermolecular interactions in crystal packing has often been at the center of a lively debate in the crystallographic community.[7–9]

High-pressure studies could be exploited to shed more light on weak interactions, because compression is a way of sampling the repulsive part of the intermolecular potentials (whereas attractive forces remain elusive). Therefore, in the quest for increasing our knowledge on the plethora of intermolecular interactions in crystals, high pressure (HP), better than low temperature, can be an effective probing tool. For instance, the effects of pressure on intermolecular forces hierarchy were observed in recent works on halogenated molecules, high-

lighting the competition between X$\cdots$X and C—H$\cdots$X contacts.[10,11]

Indeed, the compressibility of different interactions clarifies the role played by them in the crystal packing; moreover, although they do not directly induce cohesion, at extreme conditions minimization of the repulsion is the driving force of polymorphism or chemical reactions. Since the stronger interactions are usually retained in the different polymorphs of molecular crystals, the weaker forces are often the determining ones in provoking phase transitions.[12]

Gilli and coworkers proposed a unifying scheme for all intermolecular interactions,[13] which we adopt in this work. They explained all intermolecular interactions in terms of electron donor-acceptor (EDA) interactions, classified trough the well established paradigm of frontier molecular orbitals (FMOs). Each EDA pair is seen as an incipient interaction between the highest occupied molecular orbital (HOMO) of the electron donor/nucleophile and the lowest unoccupied molecular orbital (LUMO) of the electron acceptor/electrophile. Common electron donors are lone pairs (n), bonding pairs from σ FMOs (σ), and bonding pairs from π FMOs (π); common electron acceptors are empty (and tipically antibonding) FMOs (n^*, σ^*, or π^*). With this approach, for instance, each kind of "D—H$\cdots$:A" HB is a $\sigma^* \leftarrow\!\!- n$ interaction.[13]

In this study, we focused our attention on unusual $\pi^* \leftarrow\!\!- n$ interactions between NO_2 groups. Their nature is at present still unclear. Studies performed on nitrocubanes revealed a destabilizing nature, although associated with very small energy enhancement, of perpendicularly oriented $NO_2\cdots NO_2$ contacts.[14–16] By contrast, Woźniak and coworkers suggested attractive interactions between neighboring NO_2 groups in N,N-dipicrylamine and later supported this hypothesis with theoretical calculations on HNO_2 dimer.[17–19] Recently, Daszkiewicz performed theoretical calculations on dimeric systems occurring in crystal structures as perpendicularly arranged NO_2 groups. He estimated the interaction energy of each $NO_2\cdots NO_2$ contact by dividing the total interaction energy for the number of $NO_2\cdots NO_2$ contacts and concluded that they are attractive, and comparable to weak hydrogen bonds.[20]

High pressure studies on NO_2 group containing compounds have been present in literature

for quite some time,[21–23] and they are especially common in the field of explosives and energetic materials.[24–27] Not surprisingly, $NO_2 \cdots NO_2$ interactions are often observed in the literature of this field, but they have usually been regarded as unfavorable contacts.[25,28] Recently, however, they have been indicated as possible stabilizing interactions in co-crystals of energetic materials.[29–32]

The molecule that prompted our interest in $NO_2 \cdots NO_2$ contacts is 4-amino-4′-nitrobiphenyl (44′ANBP), of which we report a previously unobserved HP polymorph, featuring a $NO_2 \cdots NO_2$ short contact. The experimental observations were complemented with periodic DFT calculations on 44′ANBP itself, on 1-hydrazino-2,2-dinitroethenamine, and on 3-nitrato-1-nitroazetidine. The latter compounds, which are unstable energetic materials,[33–35] contain several $NO_2 \cdots NO_2$ contacts with different geometrical configurations.

In order to analyze the results and better classify the nature of this interaction, we have employed several theoretical tools. Dimeric systems with different configurations were modeled *ab initio* to explore the potential energy surfaces of $NO_2 \cdots NO_2$ contacts and determine their interaction energies. The dual descriptor $f^{(2)}(r)$ was employed to analyze the electron density of such models; this reactivity index is based on Fukui functions and enables to predict the most nucleophilic and electrophilic regions of the system.[36–38] Semi-empirical pairwise atomic potential energies were computed to evaluate the contribution of each chemical moiety to the crystal packing and, more importantly, to qualitatively determine the forces associated to intermolecular contacts in the presence of external pressure. Other energy decomposition schemes, such as the one implemented in ADF[39] and Crystal Explorer,[40] were adopted to benchmark our semi-empirical calculation.

Experimental

Recrystallization

Commercial 44′ANBP (TCI ≥96% purity) was recrystallized in dichloromethane by slow solvent evaporation. The crystals present an intense orange color and a parallelepiped habit.

Data Collection at ambient pressure

A crystal of 44′ANBP (ca. 0.30 × 0.10 × 0.05 mm^3) was mounted with epoxy glue on a glass needle and the diffracted intensities were collected at 290K. The measurements were carried out with an Oxford Diffraction SuperNova area-detector diffractometer using mirror optics monochromated MoKα radiation (λ=0.71073Å). The temperature was maintained constant with a Cryostream 700 by Oxford Cryosystems. CrysAlisPro[41] was used for the data collection, data reduction, and gaussian absorption correction. The crystal structure was solved by direct methods using SHELXS-2014[42] and least-squares refined with SHELXL-2014[42] using anisotropic thermal displacement parameters for all non-hydrogen atoms.Hydrogen atoms were assigned geometrically and refined with a riding model; to each hydrogen atom was assigned a fixed isotropic displacement parameter with a value equal to 1.2U_{eq} of its parent atom.

Data Collection at different pressures

Four different crystals of 44′ANBP (ca. 0.15 × 0.10 × 0.05 mm^3) were employed to collect data at high pressure. All of them were loaded separately in a Merrill-Bassett diamond-anvil cell[43] equipped with 0.5 mm diamonds and a steel gasket, pre-indented to ∼0.80 mm and with a 0.25 mm hole diameter. Nitrogen, Daphne oil 7474, and a mixture of methanol and *n*-propanol 1:2 were used respectively as pressure transmitting media for samples **1**, **2**, and **3** - **4**. Pressure was calibrated with the ruby fluorescence method.[44,45] The diffracted intensities were collected at RT and 0.6 (sample **1**), 1.8, 2.9 (sample **2**), 3.4, 4.4, and 6.2 GPa

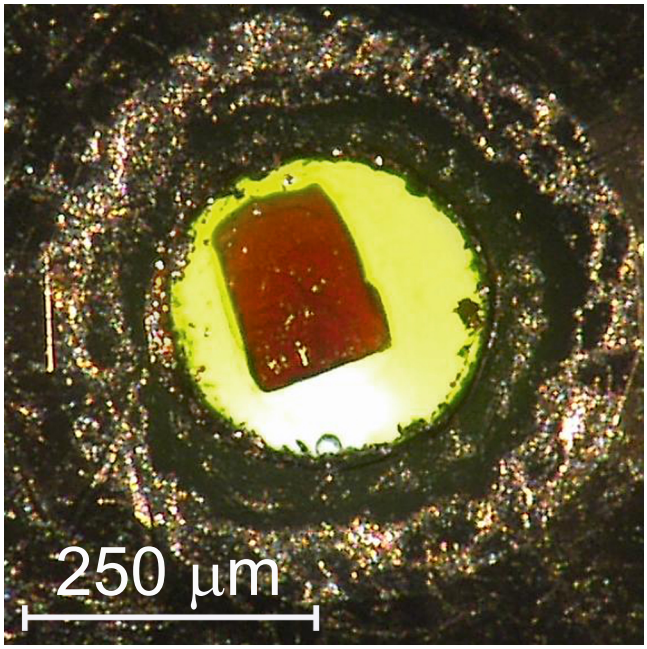

Figure 1: Sample **3** of 44′ANBP in a DAC at ∼5 GPa.

(sample **3**) with an Oxford Diffraction SuperNova area-detector diffractometer using mirror optics monochromated MoKα radiation (λ=0.71073Å). Quick experiments for cell constants determination during decompression were performed at 0.4 GPa and ambient pressure, respectively for samples **2** and **3**.

CrysAlisPro[41] was used for the data collection, data reduction, and empirical absorption correction. All crystal structures were least-squares refined with SHELXL-2014[42] using isotropic thermal displacement parameters for non-hydrogen atoms. Hydrogen atoms were assigned geometrically and refined with a riding model; to each hydrogen atom was assigned a fixed isotropic displacement parameter with a value equal to 1.2U_{eq} of its parent atom.

Sample **4** was used exclusively to determine cell constants at different pressure points around the phase transition pressure. Quick experiments were performed at 0.7, 1, 1.3, and 2.2 GPa during compression, and at 1.9, 1.5, 1.1, 0.6, 0.4, 0.1 GPa during decompression. These data collections were carried out at the X04SA Material Science beamline of Swiss Light Source (Paul Scherrer Institute, Switzerland) with a Pilatus 6M detector (λ=0.49731Å).

Table 1: Crystal Data and Refinement of 44′ANBP at different pressures.

Chemical formula, M_r (g mol^{-1}): $C_{12}H_{10}N_2O_2$, 214.22							
Pressure (GPa)	Ambient	0.6(2)	1.8(2)	2.9(2)	3.4(2)	4.4(2)	6.2(2)
Sample	**1**	**1**	**2**	**2**	**3**	**3**	**3**
Crystal system	Orthorhombic	Orthorhombic	Monoclinic	Monoclinic	Monoclinic	Monoclinic	Monoclinic
Space Group	$Pca2_1$	$Pca2_1$	$P2_1/c$	$P2_1/c$	$P2_1/c$	$P2_1/c$	$P2_1/c$
Z	4	4	4	4	4	4	4
a/Å	24.3676(8)	24.071(18)	5.6875(10)	5.6523(11)	5.570(12)	5.491(12)	5.457(7)
b/Å	5.8131(2)	5.7224(5)	6.994(10)	6.838(10)	6.8239(15)	6.7535(15)	6.5811(8)
c/Å	7.3901(2)	7.1934(5)	22.775(3)	22.599(3)	22.571(6)	22.482(7)	22.213(4)
β/°	90	90	92.650(13)	92.929(13)	93.35(6)	93.78(7)	93.95(4)
V/Å^3	1046.82(6)	990.8(8)	905.0(13)	872.3(13)	856.5(19)	831.9(18)	795.8(10)
μ (mm^{-1})	0.1	0.1	0.11	0.11	0.12	0.12	0.13
Unique reflections	2250	445	391	380	433	404	367
R_{int}	0.034	0.034	0.097	0.087	0.122	0.113	0.083
θ_{max}/°	28.2	21.9	22	21.9	22	22	21.9
R[$F^2 > 2\sigma F^2$], wR(F^2)	0.046, 0.103	0.043, 0.095	0.093, 0.278	0.089, 0.284	0.051, 0.101	0.053, 0.113	0.048, 0.100
Goodness-of-fit S	1.07	1.08	1.11	1.08	0.88	0.91	0.91
$\Delta\rho_{max}$, $\Delta\rho_{min}$(eÅ^{-3})	0.13, -0.11	0.12, -0.10	0.20, -0.23	0.25, -0.21	0.14, -0.13	0.14, -0.12	0.14, -0.15

Theoretical Calculations

Periodic DFT calculations

Periodic DFT calculations were performed with the software CRYSTAL14[46] using the hybrid functional B3LYP. Basis sets for C (6-31d1G),[47] N (6-31d1G),[47] O (6-31d1G),[47] and H (3-1p1G)[47] atoms were obtained from the CRYSTAL library. London-type pairwise empirical correction to the energy was used to account for dispersion effects.[48] Where possible, experimental XRD structure at ambient pressure was used as starting guess for geometry optimization (also at ambient pressure). The optimized structure was then used as a guess for the calculation of the next pressure point. In the case of the monoclinic phase of 44′ANBP the 1.8 GPa experimental structure was used as a guess for a 1.5 GPa geometry optimization. The optimized geometry was then used both to relax and to further increase pressure. For 44′ANBP calculations were performed at ambient pressure, 0.5, 1, 1.5, 3, 5, 10, 20, and 30 GPa in $Pca2_1$ and $P2_1/c$ space-groups. For 1-hydrazino-2,2-dinitroethenamine calculations were performed at ambient pressure, 0.5, 1, 1.5, 3, 5, 10, 15, 20, 30, 40, and 50 GPa in *Pnma* space-group. For 3-nitrato-1-nitroazetidine calculations were performed at ambient pressure, 0.5, 1, 1.5, 3, 5, 10, 15, 20, 30, 40, and 50 GPa in $P4_1$ space-group. Calculations in *P1* space-group were also performed for all compounds at different pressure to check for

the possible existence of alternative phases; PLATON[49] was used to retrieve their symmetry. Calculations of vibration frequencies for both phases of 44′ANBP were performed at ambient pressure, 0.25, 0.5, 1, 1.5, and 3 GPa. Gibbs free energy at 298.15 K was then computed as follows:

$$\Delta G = \Delta H - T\Delta S \cong (E_{DFT} + E_{dp} + E_0 + E_T) + P\Delta V - T\Delta S \quad (1)$$

Where E_{DFT} is the electronic energy from the periodic DFT calculation, E_{dp} is the correction for dispersive effects, E_0 is the zero-point energy, and E_T is the thermal contribution to the vibrational energy.

Gas-phase calculations

Gas-phase calculations were performed with the software GAUSSIAN09.[50] Calculations for estimation of dipole moments and polarization were carried out at the B3LYP//6-31G(d,p) level. All calculations on the dimeric models were instead carried out at the MP2//6-311+G(d,p) level. The $NO_2\cdots NO_2$ (∥A, ∥S, ⊥AP, ⊥AC, ⊥SC, ⊥SP) and $NH_2\cdots NO_2$ (symmetric bifurcated: AC, SC, AP=SP; asymmetric bifurcated and monofurcated -AC, +AC, AP, -SC, +SC, SP) idealized models were constructed with pre-optimized molecules of nitrobenzene and aniline. The PESs for the $NO_2\cdots NO_2$ idealized models were calculated along the N—O$\cdots$N distance for the range from 3 to 5 Å, with a stepsize of 0.1 Å. For the $NH_2\cdots NO_2$ the distance range used was from 1 to 5 Å, with the same stepsize; the selected distances were N—H$\cdots$O for the monofurcated and asymmetric bifurcated cases and N—H$\cdots$H for the symmetric bifurcated. Interaction energies for dimeric $NO_2\cdots NO_2$ models were calculated accounting for basis-set superposition error with the Counterpoise method at the MP2//6-311+G(d,p) level. Furthermore, ADF was used to perform an energy decomposition analyses of the $NO_2\cdots NO_2$ models and 44′ANBP dimers interaction energies at the B3LYP-D//aug-TZVP level.

Dual descriptor analysis

The wavefunctions of anion (N+1), cation (N-1) and neutral structure (N) were computed with GAUSSIAN09[50] at the MP2//6-311+G(d,p) level. The following formula was employed to compute the dual descriptor index.[37,38]

$$f^{(2)} = f_+(r) - f_-(r) = (\rho_{N+1} - \rho_N) - (\rho_N - \rho_{N-1}) \tag{2}$$

Extraction of electron densities from the wavefunctions and subsequent arithmetic operations were performed with Multiwfn 3.3.9.[51]

Semi-empirical energy breakdown

A simple semi-empirical interaction potential was computed as follows for the most important intermolecular EDA interactions:

$$V_{rep} = \sum_{ij} B_{ij} e^{-C_{ij} r_{ij}} \tag{3}$$

$$V_{disp} = \sum_{ij} -\frac{s_6 C_6^{ij}}{r_{ij}^6 [1 + e^{-d r_{ij}/(R_r^{ij} - 1)}]} \tag{4}$$

$$\begin{aligned} V_{es} = & \sum_{ij} \frac{Z_i Z_j}{r_{ij}} \\ & - \sum_{ij} \frac{Z_i (Z_j - q_j)(1 - e^{-a_j r})}{r_{ij}} \\ & + \sum_{ij} \frac{Z_j (Z_i - q_j)(1 - e^{-a_i r})}{r_{ij}} \\ & + \sum_{ij} \frac{(Z_i - q_j)(Z_j - q_j)(1 - e^{-\beta_i r})(1 - e^{-\beta_j r})}{r_{ij}} \end{aligned} \tag{5}$$

Where i and j are the atom indexes and r the distance between them. Equation 3

accounts for repulsive energy and uses the parametrization used by Williams and Cox for O,[52] N, C, and H bonded to carbon atoms.[53] For H atoms bonded to polar atoms the reparametrization by Coombes *et al.* was employed;[54] here $B_{ij} = b_i b_j$ and $C_{ij} = c_i + c_j$. Equation 4 accounts for dispersive energy using the pairwise empirical model proposed by Grimme;[48] here $C_6^{ij} = \sqrt{C_6^i C_6^j}$ and $R_r^{ij} = R_{VdW}^i + R_{VdW}^j$. Equation 5 accounts for electrostatic energy; it consists in a simple Coulombic expression corrected for taking into account the penetration energy, according to the methods described by Piquemal and coworkers.[55] The charges were obtained with a multipolar expansion of the electrostatic potential from the previously calculated B3LYP//6-31d1G wavefunctions.

The total potential energy is given by the sum of the previously described contributions:

$$V_{int} = V_{rep} + V_{disp} + V_{es} \tag{6}$$

The forces were calculated by derivation of equation 6.

Results and discussion

The phase transition in 44′ANBP

44′ANBP is a polar molecule consisting of both electron donor and electron acceptor functional groups that communicate trough a conjugated system. As common for biphenyls, in gas-phase the two aromatic rings form an angle of 35.2° due to steric repulsion of the hydrogen atoms in ortho positions. At B3LYP//6-31G(d,p) level of theory, the molecular dipole moment estimated from summation of atomic contributions computed with Quantum Theory of Atoms in Molecules (QTAIM), as implemented in AIMALL,[56] is of $\mu = 8.1$ D. The molecular volume estimated from electron density (at 0.0004 a.u.) is 307.5 Å^3, resulting in a polarization of 0.09 C/m^2.

At ambient conditions, 44′ANBP crystallizes in the orthorhombic polar space group $Pca2_1$

(a=24.3676(8) Å, b=5.8131(2) Å, c=7.3901(2) Å). In the crystal structure the molecule assumes a planar conformation with a molecular volume of 261.7 $Å^3$ (obtained dividing the experimental unit cell volume by the Z value) and a dipole moment of $\mu = 7.1$ D, estimated from summation of atomic dipole moments computed with QTAIM for periodic structures at B3LYP//6-31G(d,p) level (as implemented in TOPOND14[47]). The resulting molecular polarization is slightly smaller (0.09 C/m^2). The crystal packing, however, is such that the molecular dipoles are almost antiparallel to each other and therefore the resulting crystal polarization is much lower (0.005 C/m^2).

The X-ray crystallographic structure determined at room temperature (RT) is in good agreement with the previously reported one.[57] Along the **a** axis, the molecules are disposed in a staggered head-to-tail arrangement that generates distinct hydrophobic and hydrophilic regions (Figure 2). A zig-zag chain of N—H$\cdots$O $\sigma^* \longleftarrow n$ ($NH_2 \cdots NO_2$) is visible along the **b** axis, forming a two-dimensional sheet due to the glide plane perpendicular to that direction. Oxygen atoms in NO_2 groups are known to be poor hydrogen bond acceptors. In fact, the resonant forms of the group address only a partial charge to the oxygen. Moreover the electronegativity of nitrogen is larger with respect to (for example) that of carbon. Therefore, HBs at NO_2 are generally weak and do not show strong directionality. In fact, bifurcated interactions (symmetric or asymmetric) with amino group hydrogen atoms are more common than monofurcated ones.[58] In this case, the interactions in the zig-zag chain alternate between a seemingly asymmetric bifurcated and a monofurcated one. Perpendicularly to this chain and along the **c** axis, molecules are arranged in a head-to-head fashion, so that the NO_2 groups face each other while lying on parallel planes. The O$\cdots$N distances are of $\sim$3.6 Å, but the groups are not well aligned, with a N—O$\cdots$N—O torsion of $\sim$33°. NO_2 groups are also known to interact with aromatic rings trough $\pi^* \longleftarrow n$ interactions,[59,60] but in this case the possibility is geometrically precluded.

As expected from known data at 90 K,[61] on lowering the temperature no significant changes occur to the structure of 44′ANBP, as well as on increasing it to 330 K. By contrast, upon in-

creasing the pressure up to 1.3 GPa, a first order phase transition occurs, leading to the monoclinic centrosymmetric space group $P2_1/c$ (a=5.7355(8) Å, b=7.1002(5) Å, c=22.884(18) Å, β=92.44(2)°). As a consequence of the symmetry reduction, a splitting into two twin domains was observed.

Interestingly, a center of inversion is generated during the transition, leading to a centrosymmetric and therefore perfectly non-polar structure. The molecular dipole moments, after a sliding of the molecular planes, become perfectly antiparallel and cancel each other out (Figure 2).

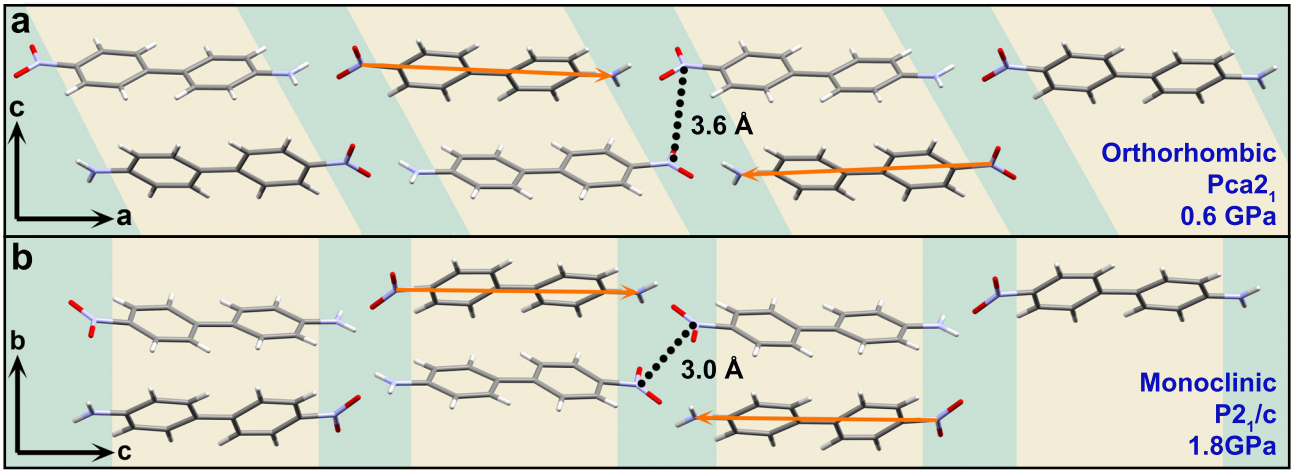

Figure 2: Phase transition of 44′ANBP; green and yellow background indicates respectively hydrophilic and hydrophobic regions. A scheme of dipole moments arrangement is portrayed by the orange arrows. Distances between centroids of nitro groups are highlighted.

Gibbs free energy calculations performed on the two polymorphs revealed that the monoclinic phase becomes energetically favored already at 0.25 GPa (at T = 298 K; see SI), despite the orthorhombic being still observed experimentally until 1 GPa. The phase transition is reversible and hysteresis was observed, with the crystal being still in the monoclinic phase at 0.4 GPa during the decompression (Figure 3).

The zig-zag chain of N—H$\cdots$O $\sigma^*\longleftarrow n$ ($NH_2\cdots NO_2$) is retained in the new polymorph along the **a** axis. Additionally, along the **b** axis, N—H$\cdots$N $\sigma^*\longleftarrow n$ interactions between amino groups of neighboring molecules are now observable. In the same direction, the NO_2

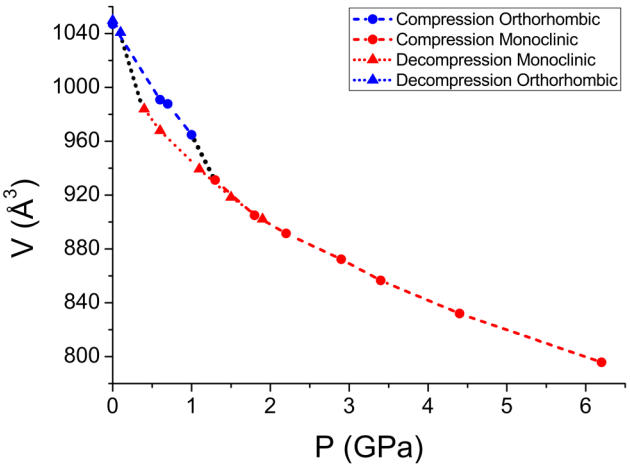

Figure 3: Volume of 44′ANBP unit cell under pressure. Black dotted lines represent the phase transition pressure ranges during compression and decompression.

groups opposing each other and lying on parallel planes are now closer (∼3 Å) and perfectly aligned (with N—O···N—O mean planes angle of 0° dictated by the new center of inversion). Figure 4 shows the molecule-molecule interaction energies computed with Tonto at the B3LYP/6-31G* level as implemented in CrystalExplorer17.[40] In both polymorphs, the most stabilizing interactions for the packing at ambient pressures are the π stacking interactions. This is especially true for the ones where the molecular dipole moments are oriented in opposite directions, showing that, despite their nature being mainly dispersive, the electrostatic contributions are non-negligible. These contacts, however, turn to be the most repulsive ones at higher pressures, with hydrogen bonds becoming the most stabilizing interactions. With this approach, of course, we cannot extract the contribution of each individual functional group to the total interaction energy; however, in both polymorphs, the interactions containing the NO_2-NO_2 contacts show mostly small attractive energies in the considered pressure range. Indeed, this interactions only become repulsive at very high pressure (20 GPa, calculated) in the monoclinic phase; the increase of the repulsive contribution due to the shortening of the distances is counterbalanced by a decrease of the dispersive and electrostatic contributions.

These results render a picture of the first shell of interactions in the crystal packing, which

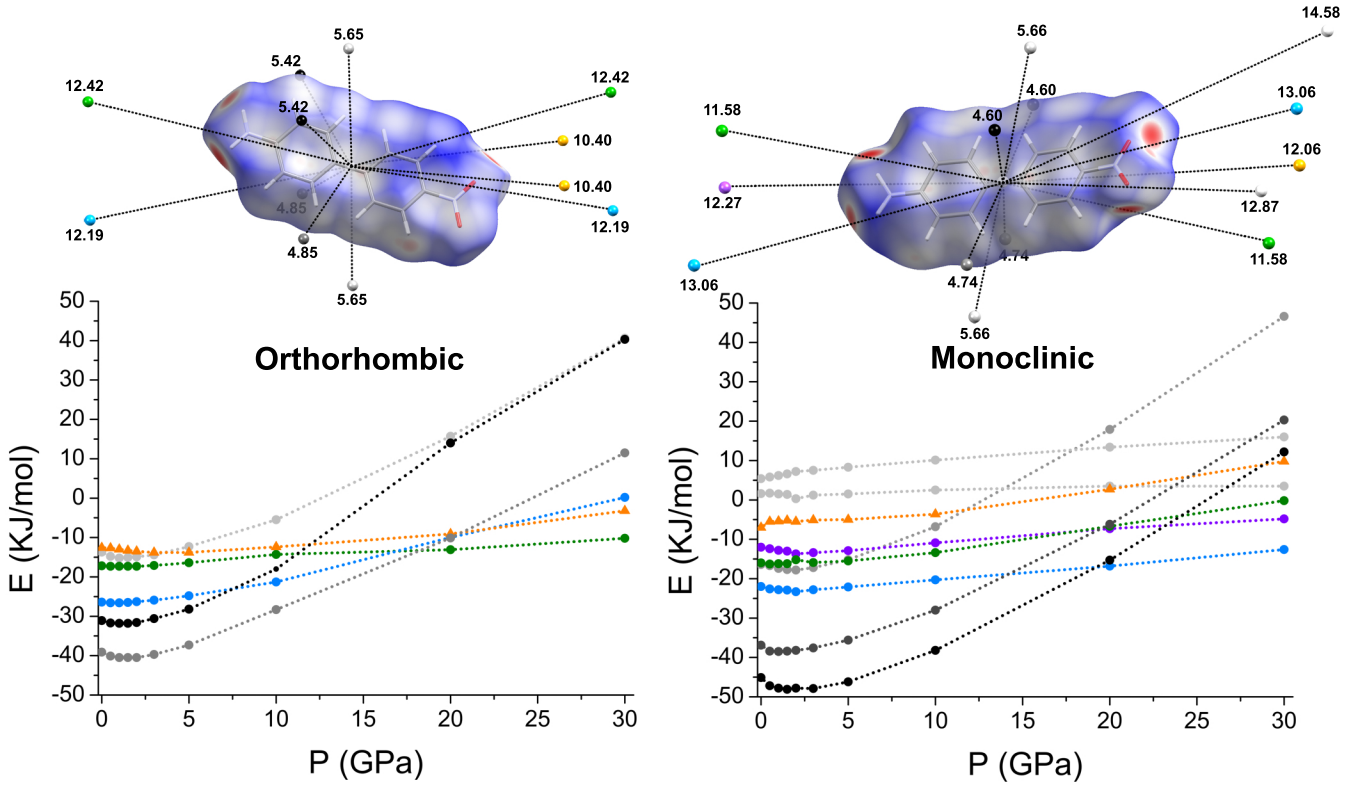

Figure 4: d_{norm} Hirshfeld surface and energies of molecule-molecule interactions computed with Tonto at the B3LYP/6-31G* level as implemented in CrystalExplorer17; distances between the centroids of involved molecules are reported in Å. Orange with triangles = NO_2-NO_2, green = monofurcated NH_2-NO_2, blue = bifurcated NH_2-NO_2, purple = NH_2-NH_2, greyscale = π stacking interactions.

is responsible for the arrangement of the molecules. However, the sum of all the interaction energies of each polymorph fails to address the crossover between lattice energies of the two polymorphs at high pressure. Indeed the orthorhombic phase would seem the most stable at every pressure, which is in contradiction with the results we obtained from the Gibbs free energy calculations and suggests that the sum of many smaller longer-range contributions in the periodic lattice could be responsible for the stabilization of the monoclinic phase.

The $NO_2 \cdots NO_2$ packing motifs

Although $NO_2 \cdots NO_2$ interactions are not much discussed in the literature, more than 4500 structures in the Cambridge Structural Database[62] contain contacts between oxygen and nitrogen atoms from nitro groups which are shorter than the sum of the Van der Waals radii. Figure 5 shows an idealization of the most frequent configurations for these contacts; the NO_2 groups may lie on parallel planes with an anti ($\|$A) or syn ($\|$S) reciprocal orientation, or in perpendicular planes, where the possible orientations are antiperiplanar ($\perp$AP), anticlinal ($\perp$AC), synclinal ($\perp$SC), and synperiplanar ($\perp$SP). The contacts of 44′ANBP are of the $\|$A kind.

Periodic DFT calculations were performed for both polymorphs of 44′ANBP at different pressures (up to 30 GPa) and are in good agreement with the available experimental data; this not only allowed us to obtain information for a larger pressure range, but also ensures full comparability.

In Figure 6, we report the compression of selected intermolecular distances from the aforementioned EDA interactions of both polymorphs. At least one $O \cdots N$ contact in $NO_2 \cdots NO_2$ interaction seems to be a preferential pathway for compression until 10 GPa; this behavior is especially evident in the monoclinic phase and the question arises to whether the shortening of this intermolecular distance is the cause of the phase transition or merely one of its effects. To further investigate the behavior of $NO_2 \cdots NO_2$ interactions under pressure, 1-hydrazino-2,2-dinitroethenamine and 3-nitrato-1-nitroazetidine, two compounds that contain several

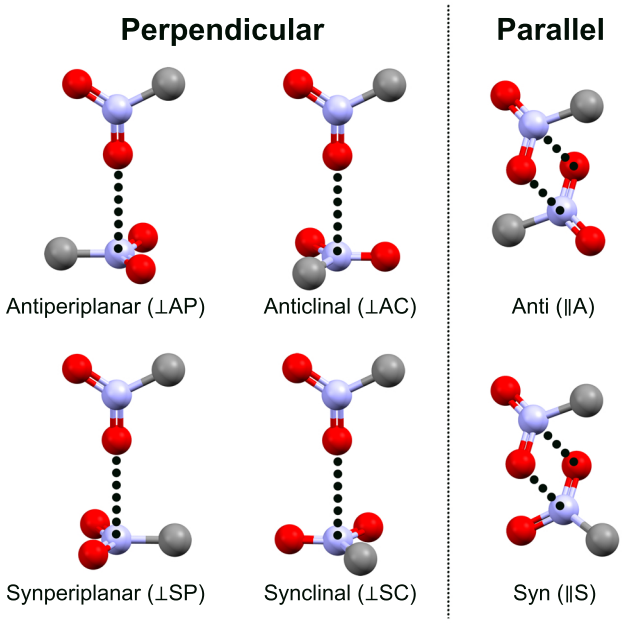

Figure 5: Idealized models of the most frequent configuration of $NO_2 \cdots NO_2$ interactions.

$NO_2 \cdots NO_2$ with complementary characteristics (namely parallel and perpendicular contacts), were also studied computationally with periodic-DFT simulations.

1-hydrazino-2,2-dinitroethenamine, a derivate of the explosive FOX-7,[63] crystallizes in the orthorhombic space group *Pnma*.[64] The amino and hydrazino groups lie on the same plane; the two symmetry equivalent nitro groups lie on a plane perpendicular to it. Two kinds of symmetry unique $NO_2 \cdots NO_2$ short contacts are present: one features a perpendicular orientation of the nitro groups (red in Figure 7a) and the other a parallel one (yellow in Figure 7a). Several N—H$\cdots$O $\sigma^* \leftarrow\!\!- n$ are also observable between the amino and hydrazino hydrogen atoms and the nitro oxygen atoms. It is noteworthy to mention that a different structure for 1-hydrazino-2,2-dinitroethenamine in P-1 space group, with pyramidal nitrogen atoms in NH_2 groups, was computationally identified at 30 GPa. This alternative structure, seems to be more stable than the planar one, but convergence could not be reached, indicating that the minimum could be very shallow. The possible existence of a more stable conformation could be speculated also for lower pressures, with the experimentally determined one being the average structure between two conformations.

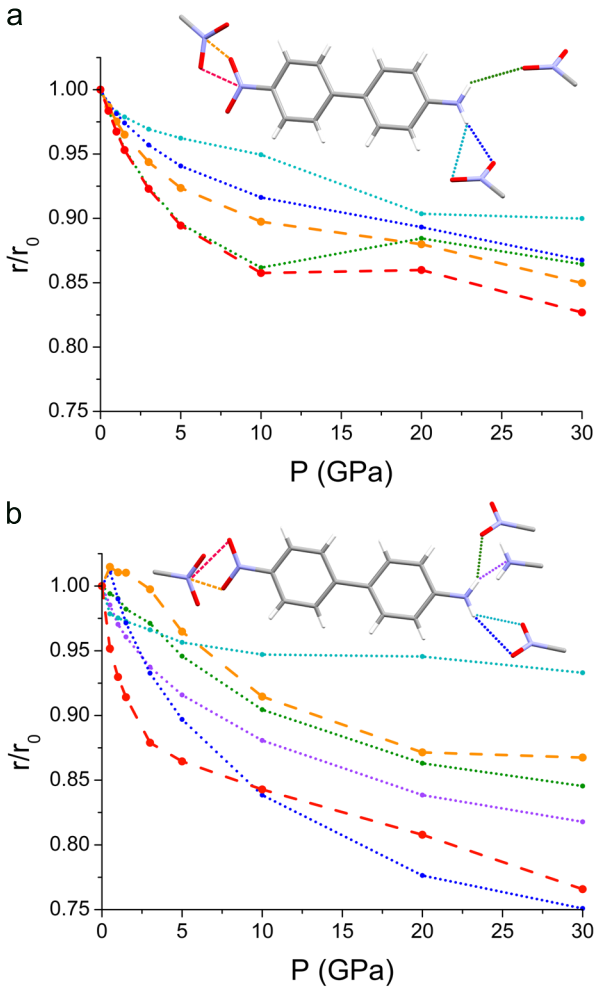

Figure 6: Relative shortening of distances involved in selected EDA interactions of both polymorphs of 44′ANBP. The curves were obtained using periodic DFT calculated distances at 0, 0.5, 1, 2, 3, 5, 10, 20, and 30 GPa;(**a**) orthorhombic phase; (**b**) monoclinic phase.

3-nitrato-1-nitroazetidine crystallizes in the tetragonal space group $P4_1$.[65] The four membered ring is considerably tilted with an angle of 12.7° between the C—N—C and the C—C—C planes; the azetidine nitrogen presents pyramidal geometry and the nitro and nitrato groups are on opposite sides with respect to the ring. The O$\cdots$N distance between nitrato groups is merely of ∼2.9 Å, but the configuration is not parallel nor perpendicular (red in Figure 7b). A perpendicular interaction is observable between neighboring nitro groups (dark red in Figure 7b) and a parallel one between nitro and nitrato groups (yellow and orange in Figure 7b). Furthermore, several C—H$\cdots$O $\sigma^*\longleftarrow n$ are present in the crystal structure. Figure 7 shows the compression of selected intermolecular distances from 1-hydrazino-2,2-dinitroethenamine and 3-nitrato-1-nitroazetidine. In both cases no preferential pathway for compression towards $NO_2\cdots NO_2$ interactions was observed. The compressibility of $NO_2\cdots NO_2$ $\pi^*\longleftarrow n$ interactions seems however to be comparable to that of N—H$\cdots$O and C—H$\cdots$O $\sigma^*\longleftarrow n$ interactions.

To better understand why the $NO_2\cdots NO_2$ contacts are the most compressible in 44′ANBP, three computational methods were employed: the modeling of idealized $NO_2\cdots NO_2$ and $NH_2\cdots NO_2$ dimeric models, the semi-empirical energy breakdown with a pairwise atomic potential, and the electron density analysis with the dual descriptor.

Ab initio potential and Fukui functions for dimeric models

For the $NO_2\cdots NO_2$ idealized cases the ∥A, ∥S, ⊥AP, ⊥AC, ⊥SC, and ⊥SP configurations were modeled using a dimer of nitrobenzene. The *ab initio* potential energy surfaces (PESs) clearly show that the interactions where the NO_2 groups lie on parallel planes are more stable at longer distances, but their repulsive part of the curve starts earlier and is steeper than that of the perpendicular conformations (Figure 8a). This seems to confirm the observed trend of perpendicular $NO_2\cdots NO_2$ interactions being more compressible than the parallel ones.

For the $NH_2\cdots NO_2$ PESs (Figure 8b) only average potential energy surfaces of the 3 main

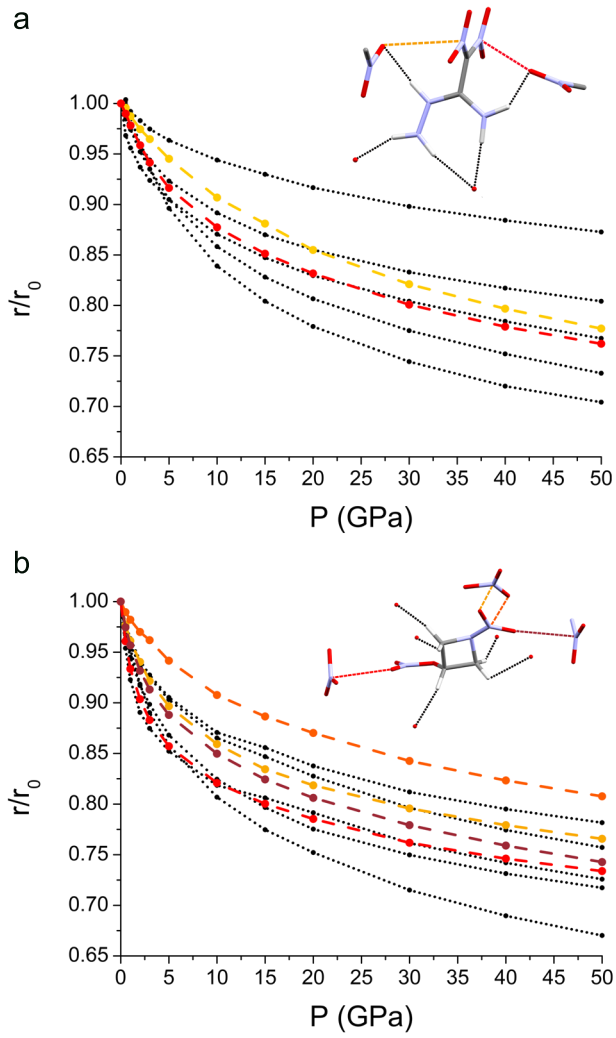

Figure 7: Relative shortening of distances involved in $NO_2 \cdots NO_2$ interactions with respect to those involved in hydrogen bonds for 1-hydrazino-2,2-dinitroethenamine (**a**) and 3-nitrato-1-nitroazetidine (**b**). The curves were obtained using periodic DFT calculated distances at 0, 0.5, 1, 2, 3, 5, 10, 20 ,30, 40, and 50 GPa.

configurations are here reported (complete information can be found in the SI); the symmetric bifurcated is an average of the AC, SC and AP(=SP) conformations, while asymmetric bifurcated and monfurcated cases are an average of -AC, +AC, AP, -SC, +SC, and SP ones. As expected the bifurcated interaction is more stable than the monofurcated, however the symmetric bifurcated one becomes significantly more destabilizing at medium-short distance range because of the larger repulsion. The asymmetric bifurcated and monofurcated interactions are more similar: in the long distance range the former is still slightly more stable, but it also becomes slightly more repulsive for short distances.

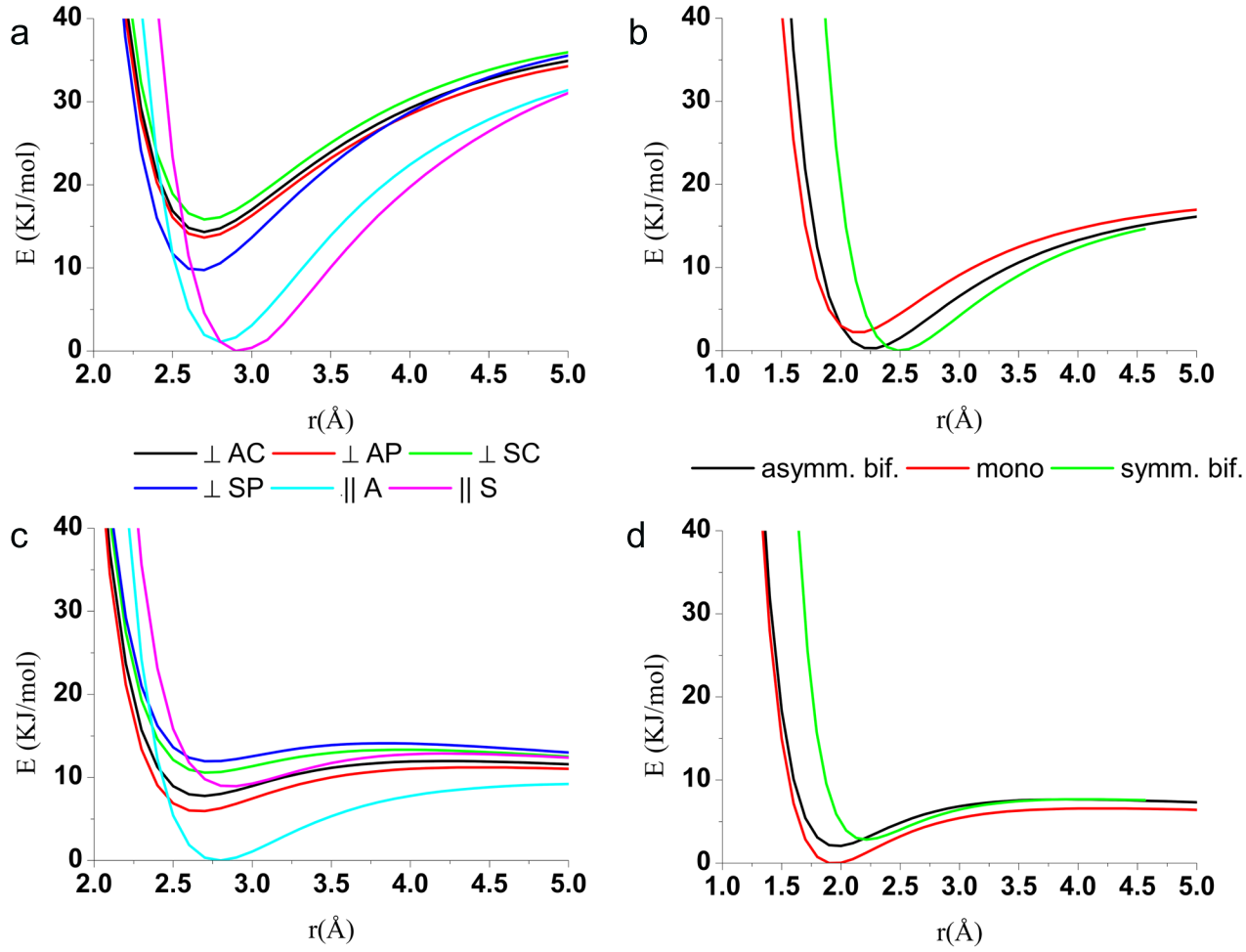

Figure 8: PESs of the idealized dimeric models; values of y-axis are calculated as relative differences to the lowest energy minimum. **a**. *Ab initio* potential for $NO_2 \cdots NO_2$ interaction. **b**. *Ab initio* potential for $NH_2 \cdots NO_2$ interaction. **c**. Semi-emprical potential for $NO_2 \cdots NO_2$ interaction. **d**. Semi-empirical potential for $NH_2 \cdots NO_2$ interaction.

The dimeric models were also used to perform an electron density analysis with Fukui functions.[36] Specifically, we computed the dual descriptor $f^{(2)}(r)$, a local reactivity index that has been successfully used in predicting the regions of a system most likely to undergo nucleophilic and electrophilic attack.[37,38] We used this approach to investigate the stabilizing or destabilizing nature of $NO_2 \cdots NO_2$. The results from the dimeric nitrobenzene models

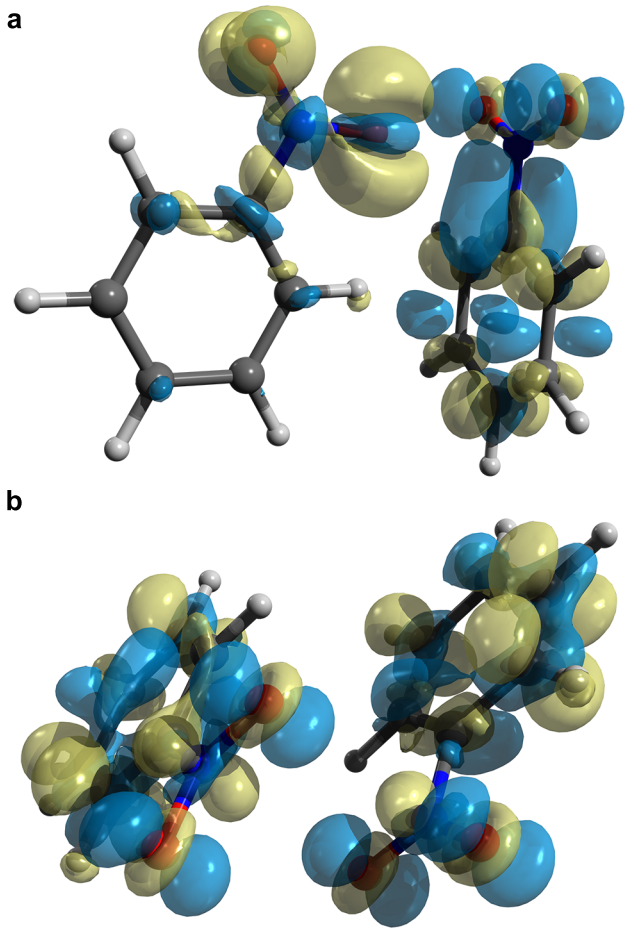

Figure 9: Dual descriptor $f^{(2)}(r)$ for $NO_2 \cdots NO_2$ interactions in $\perp$SP (**a**) and $\|$S (**b**) models; blue and yellow regions highlight respectively the most electrophilic and the most nucleophilic parts of the system. Graphic elaboration performed with isovalue=0.005 a.u. in Avogadro.[66]

(Figure 9) clearly show that this interaction is indeed stabilizing from an orbitalic point of view. A confirmation of this observation in also given by the total orbital interactions calculated with ADF energy decomposition analysis,[39] which are all stabilizing contributions to the total interaction energies.

Table 2: Total Orbital Interaction for the idealized models of $NO_2 \cdots NO_2$ contacts computed with ADF energy decomposition analysis at the B3LYP-D//aug-TZVP level.

Model	Orb. Int. (KJ/mol)
$\perp$AC	-6.9
$\perp$AP	-6.8
$\perp$SC	-7.5
$\perp$SP	-9.3
$\parallel$A	-10.2
$\parallel$S	-13.6

Interaction energies and energy breakdown

Another strong indication that $\pi^* \longleftarrow n$ interactions between NO_2 groups could be attractive is given by the interaction energies reported in Table 3.

Table 3: Basis-set superposition error (BSSE) corrected interaction energies (E_{int}) in KJ/mol for the idealized models of $NO_2 \cdots NO_2$ contacts at the minima of their PESs (MP2//6-311+G(d,p) level); the same kind of calculation was repeated with benzene dimers, maintaining the rings position fixed, in order to evaluate the contribution of the phenyl rings to the total E_{int}.

Model	Nitrobenzene dimer E_{int} (KJ/mol)	Benzene dimer E_{int},(KJ/mol)
$\perp$AC	-9.3	-1.8
$\perp$AP	-10.2	-1.5
$\perp$SC	-6.2	-3.7
$\perp$SP	-9.3	-9.2
$\parallel$A	-13.6	-2.9
$\parallel$S	-11.2	-5.9

Although these values do not consider the contribution of other possible forces, they suggest a small stabilizing nature for all these interactions. Furthermore, to ascertain that the stabilizing effect was not due only to dispersive interactions between the phenyl rings, for every model calculations were repeated using benzene dimers instead of nitrobenzene ones (maintaining the rings position fixed). For all cases, except the $\perp$SP, the stabilizing effect is significantly larger for the nitrobenzene dimer.

The computation of a semi-empirical pairwise atomic potential energy, although rudimentary and less accurate than quantum mechanical calculations, allows us to extract the contribution

of individual functional groups from the total interaction potential between two molecules. The trend of the *ab initio* calculations on the $NO_2 \cdots NO_2$ models is not fully reproduced in the attractive regions of the PESs, whereas the pairwise potential performs better in the repulsive regions (Figure 8c-d). This is likely due to the difficulty of describing dispersive forces correctly. Nevertheless, this quantitative discrepancy does not affect significantly the qualitative picture. Furthermore, the parameters used to calculate the pairwise potential are obtained empirically from crystal structures, while we are comparing its results to gas-phase calculations.

Taking these considerations into account, and since at HP we explore the system mainly within the repulsive part of the interaction potential, we can safely use the pairwise atomic potential to evaluate the relative differences between the EDA interactions of both polymorphs of 44′ANBP, and draw at least a qualitative picture of the forces at play. Indeed, even if the semi-empirical pairwise potential does not perform so well as other methods for calculating molecular interaction energies (see SI), it allows to easily obtain the analytical derivatives of the interaction potentials with respect to the distance. Furthermore, in cases where a part of a molecule should be the main responsible for a certain interaction energy, this tool would easily allow to employ a functional group approach to speed up the calculation.

In Figure 10 the forces, *i.e.* the inverse of the aforementioned derivatives, are reported at different pressures; these forces are the vectorial response to pressure (that can be visualized as a stress tensor) and can be used as an estimation of resistance to compression. It appears clear that the resistance to compression for the $NO_2 \cdots NO_2$ interaction is the smallest in the orthorhombic phase (*i.e.* its repulsive potential is the most shallow) and therefore it is not surprising that compression preferentially occurs along the direction of this contact. After the phase transition, however, the $NO_2 \cdots NO_2$ interaction becomes less compressible and eventually the shortening starts following alternative pathways along the $NH_2 \cdots NH_2$ and the bifurcated $NH_2 \cdots NO_2$ interactions, with the latter being instead the most desta-

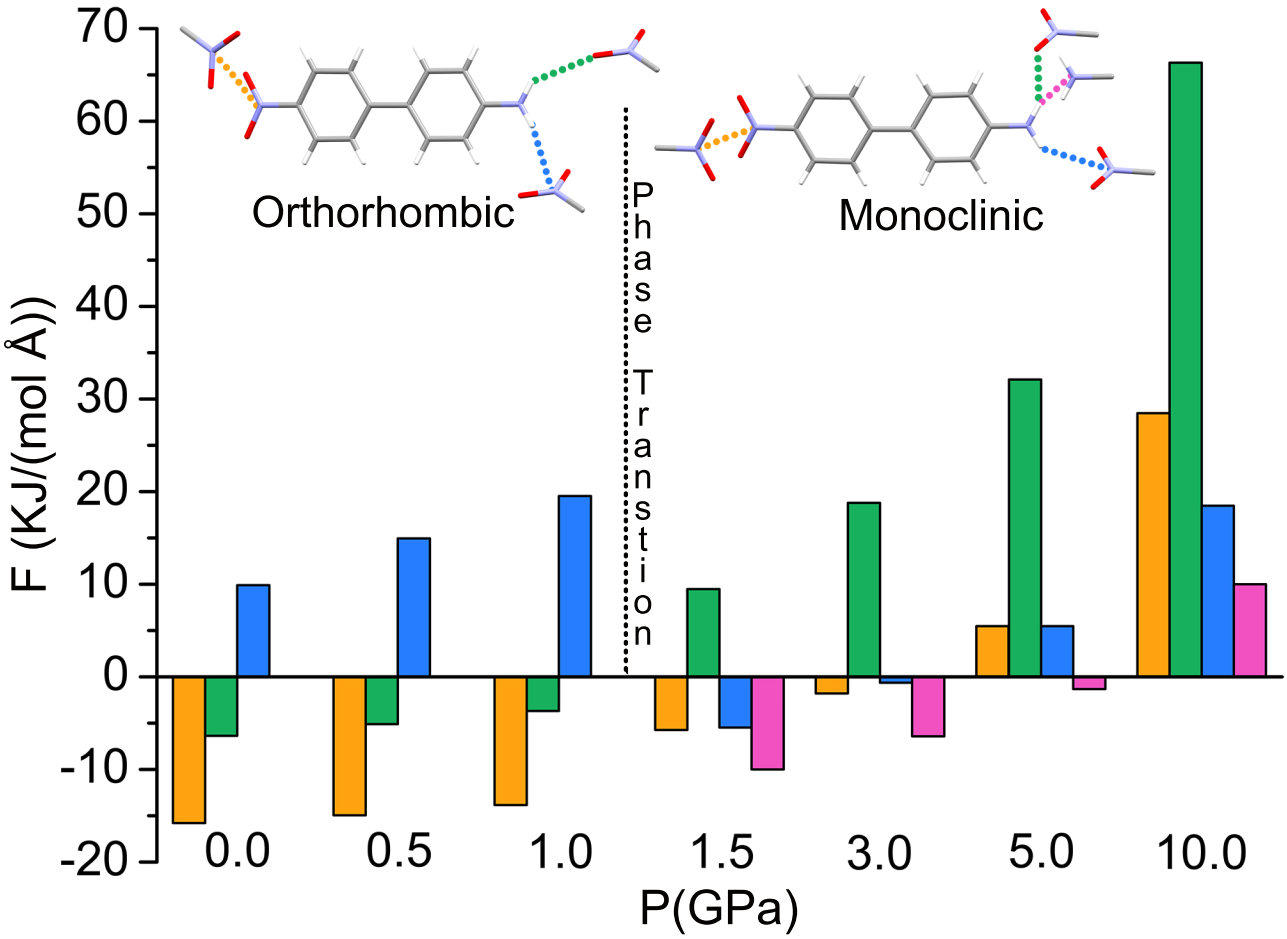

Figure 10: Forces of the main intermolecular interactions of 44′ANBP at different pressures, calculated with the semi-empirical atomic pairwise potential.

bilizing before the phase transition (because of between an amino group hydrogen and an electrophilic nitro group nitrogen in the orthorhombic phase).

Conclusions

A pressure induced phase transition was observed for 44′ANBP beyond 1 GPa, driven by the search of a closer packing in a subtle exercise of balancing intermolecular repulsive forces. A surprising observation is that $NO_2 \cdots NO_2$ contacts can be equally or even less repulsive than $NH_2 \cdots NO_2$ ones, as indicated by their compressibilities at high pressure. This observation was validated employing theoretical tools, confirming the strength of this combined approach for the study of EDA interactions.

All the results on the species under study indicate that $NO_2 \cdots NO_2$ $\pi^* \longleftarrow n$ interactions are mildly attractive at ambient conditions. However, a generalization cannot be made, because their stabilizing or destabilizing contribution may depend on specific crystal packing conditions.

At high pressure, all intermolecular interactions are frozen in a destabilizing state compensated by the external forces. Anyway, $NO_2 \cdots NO_2$ seems to minimize this unfavorable contribution. This may be useful for further investigations on explosives or high energy density materials.

The combined experimental and theoretical analysis, especially when crystals are compressed, is a valid weapon in the crystal engineer arsenal, and may help us accessing the goldmine of information necessary to classify hierarchically the many weak intermolecular interactions in crystals.

Acknowledgement

The authors thank the Swiss National Science Foundation project for supporting this study. F.M. thanks Dr.G.A. Zito for his fruitful advice regarding coding.

Supporting Information Available

The following files are available free of charge.

- SupportingInformation.pdf: Multi-Temperature SCXRD of 44′ANBP at AP, Free Gibbs energy difference between crystal phases of 44′ANBP, Gas-Phase calculations on 44′ANBP, Dual descriptor analysis of $NO_2 \cdots NO_2$ models, Gas-Phase calculations on nitrobenzene-aniline models, Evaluation of the semi-empirical pairwise potential energy calculation results.
- MultiP.cif: Structural data of 44′ANBP at different pressures.
- MultiT.cif: Structural data of 44′ANBP at different temperatures.

This material is available free of charge via the Internet at `http://pubs.acs.org/`.

References

(1) Steiner, T. The Hydrogen Bond in the Solid State. *Angew. Chem., Int. Ed.* **2002**, *41*, 48–76.

(2) Legon, A. C. Prereactive Complexes of Dihalogens XY with Lewis Bases B in the Gas Phase: A Systematic Case for the Halogen Analogue B···XY of the Hydrogen Bond B···HX. *Angew. Chem., Int. Ed.* **1999**, *38*, 2686–2714.

(3) Wang, W.; Ji, B.; Zhang, Y. Chalcogen Bond: A Sister Noncovalent Bond to Halogen Bond. *J. Phys. Chem. A* **2009**, *113*, 8132–8135.

(4) Scheiner, S. A new noncovalent force: Comparison of P···N interaction with hydrogen and halogen bonds. *J. Chem. Phys.* **2011**, *134*, 094315.

(5) Zahn, S.; Frank, R.; Hey-Hawkins, E.; Kirchner, B. Pnicogen Bonds: A New Molecular Linker? *Chem. - Eur. J.* **2011**, *17*, 6034–6038.

(6) Mani, D.; Arunan, E. The X-C···Y (X = O/F, Y = O/S/F/Cl/Br/N/P) 'carbon bond' and hydrophobic interactions. *Phys. Chem. Chem. Phys.* **2013**, *15*, 14377.

(7) Dunitz, J. D. Intermolecular atom-atom bonds in crystals? *IUCrJ* **2015**, *2*, 157–158.

(8) Thakur, T. S.; Dubey, R.; Desiraju, G. R. Intermolecular atom-atom bonds in crystals - a chemical perspective. *IUCrJ* **2015**, *2*, 159–160.

(9) Lecomte, C.; Espinosa, E.; Matta, C. F. On atom-atom 'short contact' bonding interactions in crystals. *IUCrJ* **2015**, *2*, 161–163.

(10) Podsiadło, M.; Olejniczak, A.; Katrusiak, A. Halogen···halogen contra C-H···halogen interactions. *CrystEngComm* **2014**, *16*, 8279–8285.

(11) Andrzejewski, M.; Marciniak, J.; Rajewski, K. W.; Katrusiak, A. Halogen and Hydrogen Bond Architectures in Switchable Chains of Di- and Trihaloimidazoles. *Cryst. Growth Des.* **2015**, *15*, 1658–1665.

(12) Kaźmierczak, M.; Katrusiak, A. Quantitative estimate of cohesion forces. *CrystEngComm* **2015**, *17*, 9423–9430.

(13) Bertolasi, V.; Gilli, P.; Gilli, G. Adducts of TCNQ with Neutral Nitrogen Bases. Their Rationalization in Terms of Intermolecular Charge-Transfer (CT) or Electron Donor-Acceptor (EDA) Interactions. *Cryst. Growth Des.* **2012**, *12*, 4758–4770.

(14) Eaton, P. E.; Gilardi, R. L.; Zhang, M.-X. Polynitrocubanes: Advanced High-Density, High-Energy Materials. *Adv. Mater.* **2000**, *12*, 1143–1148.

(15) Zhang, M.-X.; Eaton, P. E.; Gilardi, R. Hepta- and Octanitrocubanes. *Angew. Chem., Int. Ed.* **2000**, *39*, 401–404.

(16) Hrovat, D. A.; Borden, W. T.; Eaton, P. E.; Kahr, B. A Computational Study of the Interactions among the Nitro Groups in Octanitrocubane. *J. Am. Chem. Soc.* **2001**, *123*, 1289–1293.

(17) Woźniak, K.; He, H.; Klinowski, J.; Jones, W.; Grech, E. Attractive Inter- and Intramolecular N$\cdots$O Interactions in N,N-Dipicrylamine and Its Ionic Complexes. *J. Phys. Chem.* **1994**, *98*, 13755–13765.

(18) Platts, J. A.; Howard, S. T.; Woźniak, K. Weak intermolecular interactions between nitrogen and oxygen atoms. *Chem. Phys. Lett.* **1995**, *232*, 479–485.

(19) Woźniak, K.; Mallinson, P. R.; Wilson, C. C.; Hovestreydt, E.; Grech, E. Charge Density Studies of Weak Interactions in Dipicrylamine. *J. Phys. Chem. A* **2002**, *106*, 6897–6903.

(20) Daszkiewicz, M. Importance of O$\cdots$N interaction between nitro groups in crystals. *CrystEngComm* **2013**, *15*, 10427.

(21) Cromer, D. T.; Ryan, R. R.; Schiferl, D. The structure of nitromethane at pressures of 0.3 to 6.0 GPa. *J. Phys. Chem.* **1985**, *89*, 2315–2318.

(22) Boldyreva, E. V.; Burleva, L. P.; Burgina, E. B.; Baltachinov, V. P.; Ahsbahs, H.; Uchtmann, H.; Doulepov, V. E. Effect of high pressure on the infrared spectra of solid nitro- and nitrito-cobalt(III) ammine complexes. *Ber. Bunsenges. Phys. Chem.* **1992**, *96*, 931–937.

(23) Burgina, E.; Baltakhinov, V.; Boldyreva, E.; Stoyanov, E.; Zhanpeisov, N.; Zhidomirov, G. Effect of high pressure on the vibration spectrum of nitromethane molecules: changes in the kinematics of the vibrations as a result of the decrease in the distance between the molecules. *J. Mol. Struct.* **1993**, *296*, 53–59.

(24) Fabbiani, F. P. A.; Pulham, C. R. High-pressure studies of pharmaceutical compounds and energetic materials. *Chem. Soc. Rev.* **2006**, *35*, 932.

(25) Millar, D. I. A.; Maynard-Casely, H. E.; Kleppe, A. K.; Marshall, W. G.; Pulham, C. R.;

Cumming, A. S. Putting the squeeze on energetic materials-structural characterisation of a high-pressure phase of CL-20. *CrystEngComm* **2010**, *12*, 2524.

(26) Hunter, S.; Sutinen, T.; Parker, S. F.; Morrison, C. A.; Williamson, D. M.; Thompson, S.; Gould, P. J.; Pulham, C. R. Experimental and DFT-D Studies of the Molecular Organic Energetic Material RDX. *J. Phys. Chem. C* **2013**, *117*, 8062–8071.

(27) Hunter, S.; Coster, P. L.; Davidson, A. J.; Millar, D. I. A.; Parker, S. F.; Marshall, W. G.; Smith, R. I.; Morrison, C. A.; Pulham, C. R. High-Pressure Experimental and DFT-D Structural Studies of the Energetic Material FOX-7. *J. Phys. Chem. C* **2015**, *119*, 2322–2334.

(28) Davidson, A. J.; Oswald, I. D. H.; Francis, D. J.; Lennie, A. R.; Marshall, W. G.; Millar, D. I. A.; Pulham, C. R.; Warren, J. E.; Cumming, A. S. Explosives under pressure - the crystal structure of γ-RDX as determined by high-pressure X-ray and neutron diffraction. *CrystEngComm* **2008**, *10*, 162–165.

(29) Bolton, O.; Matzger, A. J. Improved Stability and Smart-Material Functionality Realized in an Energetic Cocrystal. *Angew. Chem., Int. Ed.* **2011**, *50*, 8960–8963.

(30) Yang, Z.; Li, H.; Zhou, X.; Zhang, C.; Huang, H.; Li, J.; Nie, F. Characterization and Properties of a Novel Energetic-Energetic Cocrystal Explosive Composed of HNIW and BTF. *Cryst. Growth Des.* **2012**, *12*, 5155–5158.

(31) Li, H.; Shu, Y.; Gao, S.; Chen, L.; Ma, Q.; Ju, X. Easy methods to study the smart energetic TNT/CL-20 co-crystal. *J. Mol. Model.* **2013**, *19*, 4909–4917.

(32) Gao, B.; Wang, D.; Zhang, J.; Hu, Y.; Shen, J.; Wang, J.; Huang, B.; Qiao, Z.; Huang, H.; Nie, F.; Yang, G. Facile, continuous and large-scale synthesis of CL-20/HMX nano co-crystals with high-performance by ultrasonic spray-assisted electrostatic adsorption method. *J. Mater. Chem. A* **2014**, *2*, 19969–19974.

(33) Axthammer, Q. J.; Krumm, B.; Klapötke, T. M. The Exciting Chemistry of 1,1-Diamino-2,2-dinitroethene and 1-Amino-1-hydrazino-2,2-dinitroethene. *J. Phys. Chem. A* **2017**, *121*, 3567–3579.

(34) Archibald, T. G.; Baum, K.; Garver, L. C. Synthesis of N-Nitroazetidines. *Synth. Commun.* **1989**, *20*, 407–411.

(35) Brill, T. B.; Oyumi, Y. Thermal decomposition of energetic materials. Part 17. A relationship of molecular composition to HONO formation: bicyclo and spiro tetranitramines. *J. Phys. Chem.* **1986**, *90*, 6848–6853.

(36) Parr, R. G.; Yang, W. Density functional approach to the frontier-electron theory of chemical reactivity. *J. Am. Chem. Soc.* **1984**, *106*, 4049–4050.

(37) Morell, C.; Grand, A.; Toro-Labbé, A. New Dual Descriptor for Chemical Reactivity. *J. Phys. Chem. A* **2005**, *109*, 205–212.

(38) Martínez-Araya, J. I. Why is the dual descriptor a more accurate local reactivity descriptor than Fukui functions? *J. Math. Chem.* **2015**, *53*, 451–465.

(39) Te Velde, G.; Bickelhaupt, F. M.; Baerends, E. J.; Fonseca Guerra, C.; van Gisbergen, S. J. A.; Snijders, J. G.; Ziegler, T. Chemistry with ADF. *J. Comput. Chem.* **2001**, *22*, 931–967.

(40) Turner, M. J.; McKinnon, J. J.; Wolff, S. K.; Grimwood, D. J.; Spackman, P. R.; Jayatilaka, D.; Spackman, M. A. CrystalExplorer17. 2017; `http://hirshfeldsurface.net`.

(41) Rigaku Oxford Diffraction, CrysalisPro Software system. 2015.

(42) Sheldrick, G. M. A short history of SHELX. *Acta Crystallogr., Sect. A: Found. Crystallogr.* **2008**, *64*, 112–122.

(43) Merrill, L.; Bassett, W. A. Miniature diamond anvil pressure cell for single crystal x-ray diffraction studies. *Rev. Sci. Instrum.* **1974**, *45*, 290–294.

(44) Mao, H. K.; Xu, J.; Bell, P. M. Calibration of the ruby pressure gauge to 800 kbar under quasi-hydrostatic conditions. *J. Geophys. Res.* **1986**, *91*, 4673.

(45) Dewaele, A.; Torrent, M.; Loubeyre, P.; Mezouar, M. Compression curves of transition metals in the Mbar range: Experiments and projector augmented-wave calculations. *Phys. Rev. B* **2008**, *78*, 104102.

(46) Dovesi, R.; Orlando, R.; Erba, A.; Zicovich-Wilson, C. M.; Civalleri, B.; Casassa, S.; Maschio, L.; Ferrabone, M.; De La Pierre, M.; D'Arco, P.; Noël, Y.; Causà, M.; Rérat, M.; Kirtman, B. CRYSTAL14: A program for the ab initio investigation of crystalline solids. *Int. J. Quantum Chem.* **2014**, *114*, 1287–1317.

(47) Gatti, C.; Saunders, V. R.; Roetti, C. Crystal field effects on the topological properties of the electron density in molecular crystals: The case of urea. *J. Chem. Phys.* **1994**, *101*, 10686.

(48) Grimme, S. Semiempirical GGA-type density functional constructed with a long-range dispersion correction. *J. Comput. Chem.* **2006**, *27*, 1787–1799.

(49) Spek, A. L. Structure validation in chemical crystallography. *Acta Crystallogr., Sect. D: Biol. Crystallogr.* **2009**, *65*, 148–155.

(50) Frisch, M. J. et al. Gaussian 09, Rev D.01. 2009.

(51) Lu, T.; Chen, F. Multiwfn: A multifunctional wavefunction analyzer. *J. Comput. Chem.* **2012**, *33*, 580–592.

(52) Cox, S. R.; Hsu, L.-Y.; Williams, D. E. Nonbonded potential function models for crystalline oxohydrocarbons. *Acta Crystallogr., Sect. A* **1981**, *37*, 293–301.

(53) Williams, D. E.; Cox, S. R. Nonbonded potentials for azahydrocarbons: the importance of the Coulombic interaction. *Acta Crystallogr., Sect. B: Struct. Sci.* **1984**, *40*, 404–417.

(54) Coombes, D. S.; Price, S. L.; Willock, D. J.; Leslie, M. Role of Electrostatic Interactions in Determining the Crystal Structures of Polar Organic Molecules. A Distributed Multipole Study. *J. Phys. Chem.* **1996**, *100*, 7352–7360.

(55) Piquemal, J.-P.; Gresh, N.; Giessner-Prettre, C. Improved Formulas for the Calculation of the Electrostatic Contribution to the Intermolecular Interaction Energy from Multipolar Expansion of the Electronic Distribution. *J. Phys. Chem. A* **2003**, *107*, 10353–10359.

(56) Keith, T. A. AIMALL (Version 14.11.23). 2014; `http://aim.tkgristmill.com/index.html`.

(57) Graham, E. M.; Miskowski, V. M.; Perry, J. W.; Coulter, D. R.; Stiegman, A. E.; Schaefer, W. P.; Marsh, R. E. Unusual structural distortions induced by charge-transfer interactions through conjugated molecules: crystal structures of $NH_2(C_6H_4)(C{\equiv}C)_n(C_6H_4)NO_2$ (n = 0-3). *J. Am. Chem. Soc.* **1989**, *111*, 8771–8779.

(58) Robinson, J. M. A.; Philp, D.; Harris, K. D. M.; Kariuki, B. M. Weak interactions in crystal engineering—understanding the recognition properties of the nitro group. *New J. Chem.* **2000**, *24*, 799–806.

(59) Huang, L.; Massa, L.; Karle, J. Calculated interactions of a nitro group with aromatic rings of crystalline picryl bromide. *Proc. Natl. Acad. Sci.* **2008**, *105*, 13720–13723.

(60) Sikorski, A.; Trzybiński, D. Networks of intermolecular interactions involving nitro groups in the crystals of three polymorphs of 9-aminoacridinium 2,4-dinitrobenzoate · 2,4-dinitrobenzoic acid. *J. Mol. Struct.* **2013**, *1049*, 90–98.

(61) Zhang, Y.; Coppens, P. Experimental Crystal Structure Determination. *CCDC* **2014**, *162608*.

(62) Groom, C. R.; Bruno, I. J.; Lightfoot, M. P.; Ward, S. C. The Cambridge Structural Database. *Acta Crystallogr., Sect. B: Struct. Sci., Cryst. Eng. Mater.* **2016**, *72*, 171–179.

(63) Bemm, U.; Östmark, H. 1,1-Diamino-2,2-dinitroethylene: a Novel Energetic Material with Infinite Layers in Two Dimensions. *Acta Crystallogr., Sect. C: Cryst. Struct. Commun.* **1998**, *54*, 1997–1999.

(64) Anniyappan, M.; Talawar, M. B.; Gore, G. M.; Venugopalan, S.; Gandhe, B. R. Synthesis, characterization and thermolysis of 1,1-diamino-2,2-dinitroethylene (FOX-7) and its salts. *J. Hazard. Mater.* **2006**, *137*, 812–819.

(65) Gilardi, R.; George, C.; Flippen-Anderson, J. L. Structure of 3-nitrato-1-nitroazetidine. *Acta Crystallogr., Sect. C: Cryst. Struct. Commun.* **1992**, *48*, 1679–1680.

(66) Hanwell, M. D.; Curtis, D. E.; Lonie, D. C.; Vandermeersch, T.; Zurek, E.; Hutchison, G. R. Avogadro: an advanced semantic chemical editor, visualization, and analysis platform. *J. Cheminf.* **2012**, *4*, 17.

For Table of Contents Use Only

$NO_2 \cdots NO_2$ contacts under compression: testing the forces in soft donor-acceptor interactions.

Fabio Montisci[1*], Arianna Lanza[1,2,3], Nicola Casati[2], and Piero Macchi[1,4*]

[1]) Department für Chemie und Biochemie, Universität Bern, Bern, Switzerland
[2]) Swiss Light Source, Paul Scherrer Institute, Villigen, Switzerland
[3]) Center for Nanotechnology Innovation, Istituto Italiano di Tecnologia, Pisa, Italy
[4]) Dipartimento di Chimica, Materiali e Ingegneria Chimica "Giulio Natta", Politecnico di Milano, Milan, Italy

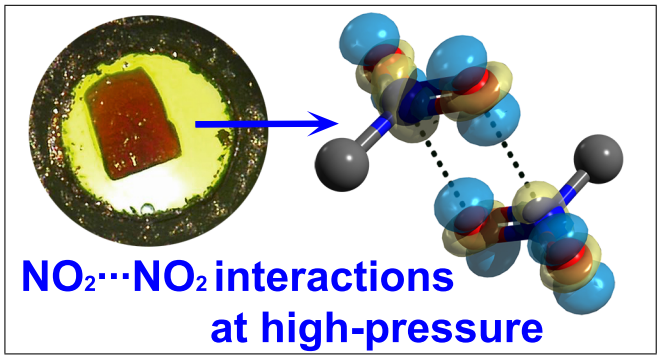

A combination of diffraction experiments at high pressure, *ab initio* calculations and theoretical tools is used to clarify the nature of nitro-nitro interactions and their role in crystal packing. A HP induced phase transition of 4-amino-4′-nitrobiphenyl is reported and characterized.